Space charge mediated negative di erential resistance in terhertz quantum well detectors

Alexandre Delga, Laetitia Doyennette, Amandine Buffaz, Vincent Berger, François-Régis Jasnot, Nicolas Péré-Laperne, Louis-Anne de Vaulchier, H.C. Liu

Space charge mediated negative differential resistance in terhertz quantum well detectors

A. Delga, L. Doyennette, A. Buffaz, and V. Berger
Université Paris Diderot, Laboratoire Matériaux et Phénomènes Quantiques, CNRS-UMR 7162, 10 rue Alice Domon et Léonie Duquet, 75205 Paris Cedex 13, France

F.R. Jasnot, N. Péré-Laperne, and L.A. de Vaulchier
Ecole Normale Supérieure, Laboratoire Pierre Aigrain, 24 rue Lhomond, 75231 Paris Cedex 05, France

H.C. Liu
Institute for Microstructural Sciences, National Research Council, Ottawa K1A 0R6, Canada

In THz Quantum Well Infrared Photodetectors, a built-in-charge-mediated regime transition of the electronic transport is thoroughly investigated. The very strong current discontinuity and negative differential resistivity behavior are explained in terms of band structure reorganizations. The analysis of bias versus current measurements reveals that the transition occurs when the first two wells of the structure become partially drained, and that second well enters the ionized regime before the first one. Both many body effects and a careful model of the contact have to be considered to account for these features. The probable source of the built-in charge is identified as Intersubband Impact Ionization, of which this regime transition would be one of the few experimental evidence, and provide an original approach to investigate hot electrons kinetics in these structures.

PACS numbers:

I. INTRODUCTION

In the electromagnetic spectrum, the terahertz region (1-10 THz) is under investigation by both optics and electronics communities[1,2]. THz efficient sources have shown a fast development, thanks to the rise of THz quantum cascade lasers[3–5]. However there is still a need for fast and high sensitive detectors, in spite of the investigation of many different devices, such as quantum dots[6], charge sensitive phototransistors[7], superconducting bolometers[8] or blocked-impurity-band detectors[9]. Although traditionally used in the near or mid-infrared regions, Quantum Well Infrared Photodetectors structures (QWIPs) have been recently investigated as another valid approach[10].

Built-in charge effects are a key factor controlling electron kinetics in semiconductors. They have a crucial -positive or negative- impact in a broad range of devices, such as double-barrier heterostructures[11], avalanche photodiodes[12,13], or solar cells[14]. In QWIPs optical gain comes from such built-in charge effects, but it has also been shown in the THz spectrum that they trigger a regime transition where the structure switches from a 'down' resistive state to an 'up' conductive state with a current discontinuity up to five orders of magnitude[15]. In this work we focus on a THz QWIP structure and we thoroughly analyze the impact of the built-in positive charges in the quantum wells with the device macroscopic behavior.

II. EXPERIMENTAL FACTS

The studied sample is a THz QWIP structure (9.7 THz) as in Ref. 10. It contains 40 GaAs quantum wells (QWs) of thickness $L_w = 11.9\,\text{nm}$ separated by wide $Al_{0.05}Ga_{0.95}As$ barriers, with $L_b = 55.2\,\text{nm}$. Each QW is doped with a nominal value of $n_{2D} = 10^{11}\,\text{cm}^{-2}$, and is designed to put in resonance both the second bound state and the bottom of the conduction band in the barriers[16]. The structure is embedded between two contacts doped up to $10^{17}\,\text{cm}^{-3}$. The performances of this detector (referred as v265) were studied by *Luo et al.*[10] between 4 and 23 K.

Figure 1 shows $I(v)$ and $V(i)$ dark characteristics measured at a temperature of 4 K. On the whole $I(v)$ curve, the bias is swept upwards then downwards, and the threshold values for the shifting up (0.84 V) is higher than the one for the shifting down (0.65 V). The hysteresis pattern is shown more clearly in the expanded scale plot. While increasing the bias from zero, the current is first dominated by interwell tunneling[15]. Temperature and bias are too low to allow electrons to flow through the continuum of states above the barriers. These channels are opened as the bias goes up, when the threshold value of 0.84 V is reached. At this stage, a sudden magnification of the process draining the QW occurs. Note that at this value, electrons injected at the contact Fermi level will have enough energy to ionize bound electrons from the wells by Coulomb interaction. A rough approximation will locate the hot electrons at an energy ΔE above the top of the barriers, where $\Delta E = E_2 - E_1 \sim 29\,\text{meV}$ is the transition energy between bound and resonant levels in the QW. Because the capture process is not en-

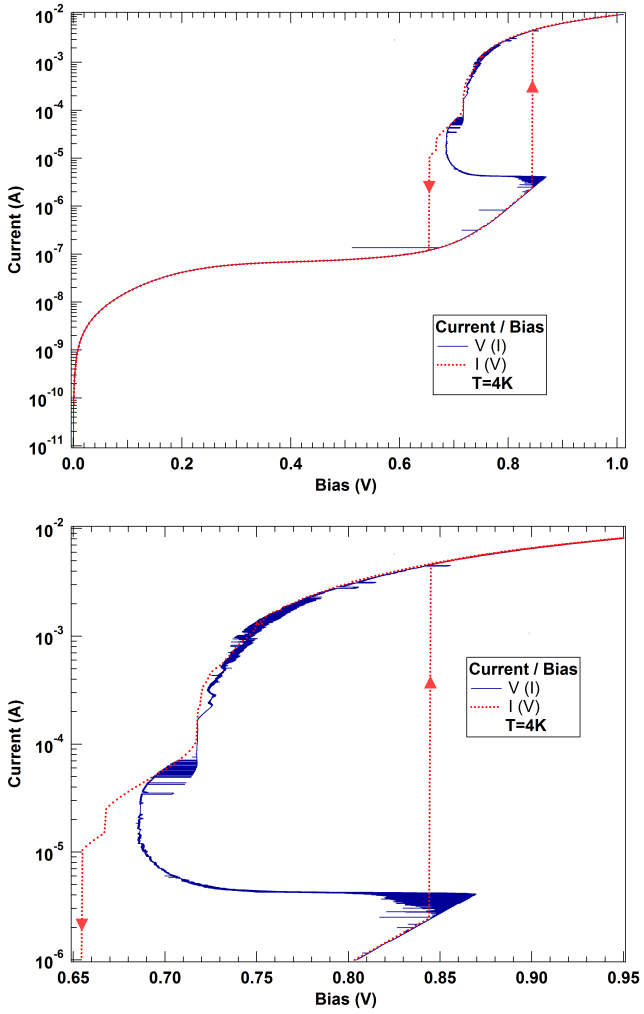

FIG. 1: $I(v)$ (dashed) and $V(i)$ (plain) dark measurements for positive bias at $T = 4\,\mathrm{K}$, for upwards and downwards sweeps. Top: whole curves. Bottom: zoom onto the hysteresis pattern. The current discontinuity reaches here three orders of magnitude, from 2.4×10^{-6} to 4.7×10^{-3} A.

hanced in the same way, some extracted electrons will leave unscreened donor impurities in the well, resulting in a built-in positive charge and an electric field discontinuity. From this point upwards the $I(v)$ and $V(i)$ curves show different behaviors. If bias is imposed, the energy difference between the two contacts is clamped. The only way for the structure to satisfy both constraints -bias and field discontinuity- is to breakdown the upstream barrier of the ionized well. This leads to a large shift of the current and the switching of the sample from the 'down' to the 'up' regime, where the current flows through the continuum of states over the barriers. On the contrary, if current is imposed, the injection field is set to a fixed value. The field discontinuity will simply lower the downstream field, and the whole 'S' pattern will be observed.

In reference 15, a qualitative interpretation of $I(v)$ measurements shows that impact ionization is responsible for the built-in charge , and that this process happens in the first wells of the structure. Two main microscopic pieces of evidence advocate for this statement. The wells in this structure are in under-populated regimes. There are fewer electrons than positive donors in the wells, which means the downstream electric field is lower than the upstream one. Hence the first wells of the structure sustain the highest fields (*i.e.* energy drops), and impact ionization is more likely to occur there. Moreover from the current level where the transition stands, an energy drop above the first period of the structure can be calculated: it is comparable to ΔE. Therefore the first wells after the contact are those involved in the regime transition. However a more quantitative theory of the built-in charge effects is needed to validate this hypothesis.

III. MODEL

The model presented here is inspired from the usual photoemissive models in QWIPs[17–20]. It is based on the fact that a macroscopic $V(i)$ curve carries all the information about a phenomenon happening above a few wells. In order to get a better insight into the physics at stake, we translated this information to a microscopic scale. Two equations can describe the behavior of one well. The field discontinuity $\mathcal{D}$ between upstream and downstream fields is linked to the well population by the Poisson equation (1). The conservation equation (2) states that in steady state the current of particles J_{in} that flows into the well equals J_{out} that flows out of it:

$$\mathcal{D} = F_{down} - F_{up} = \frac{-e(1-n)N_{dop}}{\varepsilon} \quad (1)$$

$$\frac{dn}{dt} = 0 = J_{in}(F_{up}, F_{down}, n) - J_{out}(F_{up}, F_{down}, n) \quad (2)$$

N_{dop} is the number of Si donors in a well, e the elementary charge, ϵ the dielectric permittivity, F_{up} and F_{down} the upstream and downstream electric fields, and $n = N/N_{dop}$ the relative well population ($n = 1$ when the well is neutral). These three variables $\mathcal{D}$, F_{up} and n linked by two equations can be merged into one law: $\mathcal{D} = f(F_{up})$. This discontinuity law will be the object of interest in the rest of this paper. It is indeed a direct image of the built-in charge in the ionized QW.

For a given current I flowing through the structure, it is possible to calculate the injection field $F_0(I)$ as described in section IV. The $\mathcal{D} = f(F_{up})$ law iteratively applied enables to calculate all the fields F_k along the structure, and their sum gives the bias value. Let g be the unknown function that gives $F_{down} = g(F_{up})$ ($g(x) = f(x) + x$), thus $F_k = g^{(k)}(F_0)$. We solve the functional equation:

$$V_{exp}(I) = L_b \times \sum_{k=0}^{40} g^{(k)}(F_0(I)) \quad (3)$$

It is impossible to solve (3) analytically because $V_{exp}(I)$ is extracted from experimental data. Therefore section V will be dedicated to the discontinuity law $\mathcal{D} = f(F_{up})$ through the analysis of its impact on the $V_{exp}(I)$ curve. In section VI we will present and discuss the solution obtained by numerical optimization.

IV. THE CONTACT

As shown in equation (2), an accurate model linking the current and the injection field is required. In THz QWIPs, the transition energy is around 10 meV, a value comparable to the corrections introduced by many-body interactions. *Guo et al.* showed that photoresponse peak positions cannot be explained without including their contribution[21]. Therefore it is critical to develop a good model of the band structure close to the contact. Another difficulty arises from the nature of the problem: while the contact is described by a 3D model, the quantum confinement in the wells is treated with a 2D one. This section is organized as follows. First we will determine the band structure at zero bias, by assuming that all the band structure rearrangements happen upon the first well. The criterion is that no total electric charge shall be present over the whole contact/first-well area. This will give the value $F_0(I)|_{0\mathrm{V}}$ of the injection field when no current flows through the structure. Subsequently we shall calculate the band structure and the current for different values of F_0, and use these points to interpolate the whole $F_0(I)$ law.

The effective mass $m^*(z)$ and parabolic band approximations lead to the following Schrödinger equation for the electron:

$$\left\{-\frac{\hbar^2}{2}\frac{\partial}{\partial z}\left[\frac{1}{m^*(z)}\frac{\partial}{\partial z}\right]+V(z)\right\}\varphi_l(z)=\epsilon_l\varphi_l(z) \tag{4}$$

where the total electron wave function is written as a product of a plane wave parallel to the layers, and a one-dimensional envelope function in the epitaxy growth direction z: $\psi_{l,\mathbf{k}_{/\!/}}(\mathbf{r}_{/\!/},\mathbf{z}) = e^{i\mathbf{k}_{/\!/}\cdot\mathbf{r}_{/\!/}}\varphi_l(z)$. The energy of the electron is $E_{l,\mathbf{k}_{/\!/}} = \hbar^2 k_{/\!/}^2/2m^* + \epsilon_l$, where l is the subband index. $V(z)$ is the bottom of the conduction band. The difference between 3D and 2D models lies in the way the electron density $n(z)$ is calculated. Assuming a Fermi-Dirac distribution, we write for the contact:

$$n_{3D}(z) = \frac{1}{2\pi}\left(\frac{2m^*}{\hbar^2}\right)^{3/2}\int_{\infty}^{V(z)}\frac{\sqrt{E-V(z)}dE}{1+exp\left(\frac{E-E_F}{k_BT}\right)} \tag{5}$$

with T the temperature and E_F the Fermi level. Beyond the middle of the first barrier, the density is considered two-dimensional:

$$n_{2D}(z) = \frac{m^*k_BT}{\pi\hbar^2}log\left(1+exp\left(\frac{E_F-\epsilon_l}{k_BT}\right)\right)|\varphi_l(z)|^2 \tag{6}$$

Three contributions are taken for the potential term: $V(z) = V_{QW}(z) + V_H(z) + V_{XC}(z)$. $V_{QW}(z)$ represents the potential of the quantum wells. $V_H(z)$ is the Hartree potential that accounts for the Coulomb interaction between electrons and ionized donors, and is calculated thanks to the Poisson equation:

$$\frac{\partial^2}{\partial z^2}V_H(z) = \frac{e^2}{\varepsilon}\left(N_d(z)-n(z)\right) \tag{7}$$

where ε is the dielectric constant and $N_d(z)$ the doping density. $V_{XC}(z)$ accounts for the fermionic nature of the electrons, and the many-body wave function should be written as a Slater determinant: theoretically, it cannot be factorized in one-electron wave functions. We use the local density approximation (LDA)[22] to express it:

$$\begin{aligned}V_{XC}(z) =& \frac{e^2}{4\pi^2\varepsilon a_B(z)\,r_s(z)}\left(\frac{9\pi}{4}\right)^{1/3}\\ &\times\left\{1+0.0545r_s(z)\,log\left[1+\frac{11.4}{r_s(z)}\right]\right\}\end{aligned} \tag{8}$$

with $a_B = \varepsilon\hbar^2/e^2m^*(z)$ is the effective Bohr radius and $r_s(z) = \left\{(3/4\pi)(a_B^3n(z))^{-1}\right\}^{1/3}$. The charge neutrality condition gives the last equation of this close set (eq 4-9):

$$\int_0^L\left(N_d(z)-n(z)\right) = 0 \tag{9}$$

Because of the mixed-dimensionality of the problem, a numerical method was chosen to solve it and is presented in appendix. The main physical approximation is that we do not take into account the triangular quantum confinement at the end of the contact. This condition limits the validity of this model to small electric fields, relevant in the THz range. The band structure of the contact and the first period at zero bias is shown in figure 2. Figure 3 highlights the impact of many-body effects in THz QWIPs, as previously shown in 2D calculations[21].

We use a similar method to determine the band structure for every given value of the injection field F_0. The current is given by:

$$I(F_0) = S\frac{em^*k_BT}{2\pi\hbar^3}\int_0^{\infty}D(E,F_0)\,log\left(1+e^{\frac{E_F-E}{k_BT}}\right)dE \tag{10}$$

with S the mesa area and $D(E,F_0)$ the transparency of the injection barrier calculated with a transfer-matrix method[23]:

$$\begin{aligned}D(E,F_0)^{-1} = \frac{k_{in}}{4k_{out}}&\left[\left(T_{11}+\frac{k_{out}}{k_{in}}T_{22}\right)^2+\right.\\ &\left.\left(\frac{k_{out}}{m^*}T_{12}-\frac{m^*}{k_{in}}T_{21}\right)^2\right]\end{aligned} \tag{11}$$

with k_{in} and k_{out} the wavevectors on each side of the injection barrier, and the transfer matrix coefficients are

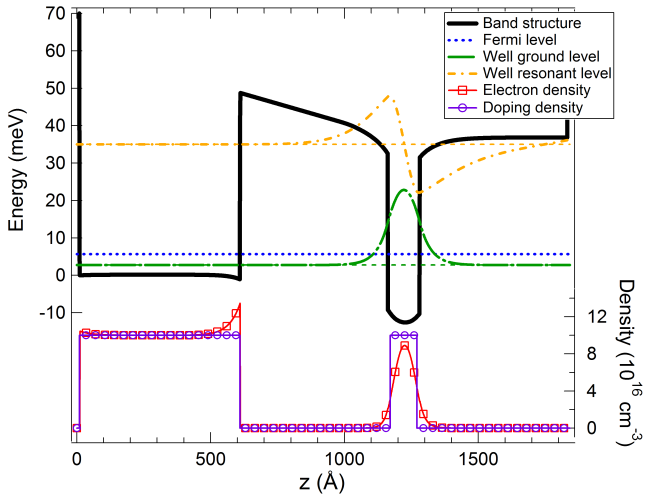

FIG. 2: Band diagram of the contact and first period of v265 calculated including Hartree and exchange-correlation corrections. At zero bias the injection field is 2.061 kV.cm^{-1}

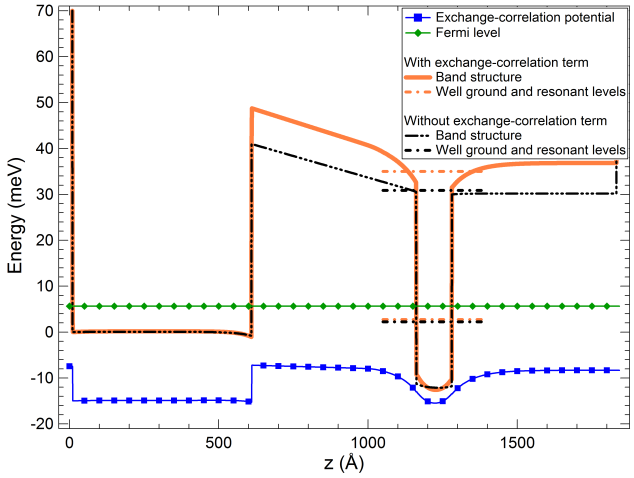

FIG. 3: Band diagram of the contact and first period of v265 calculated with and without exchange-correlation correction(V_{XC}). An error of 7.6 meV on the height of the barriers is made if V_{XC} is not taken into account. ΔE is shifted from 28.63 meV to 32.25 meV. For clarity reasons V_{XC} has been offset by -15 meV

calculated in the WKB approximation. For instance $T_{11} = \sqrt{\frac{k_{out}}{k_{in}}} cosh\left(\int_{z_{in}}^{z_{out}} k\left(z\right) dz\right)$. Because of the triangular quantum confinement, we assume that the only electrons contributing to the current are the ones whose energies are above 0, for whom the 3D model is justified. For the lower electrons, their contribution to the current is exponentially decreasing with the height of the barrier, thus is expected to be small. This will lead to a slight under-evaluation of the current. For the sake of simplicity, we also only considered the current flowing from the contact to the first well, neglecting the current going back

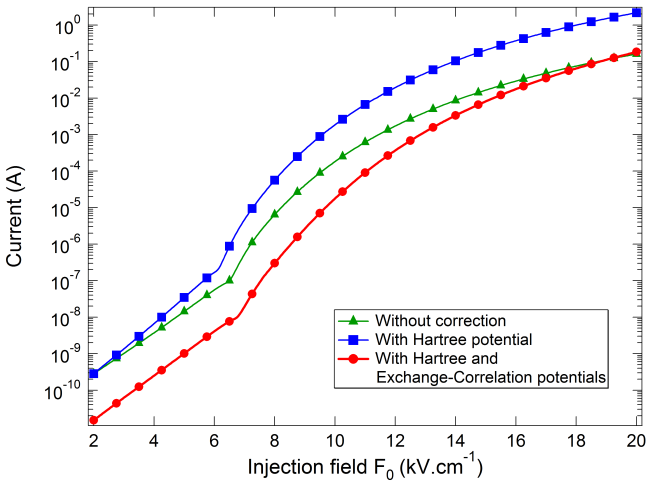

FIG. 4: $I(F_0)$ curves with three different levels of approximations. The cusps around $6-7\,\mathrm{kV.cm^{-1}}$ appear when the barrier becomes triangular.

upstream. The latter is indeed negligible as soon as the effective Fermi levels of the contact and first well are no longer aligned ($F_0 > 8\,\mathrm{kV.cm^{-1}}$), which is the range of interest. Figure 4 plots the current versus injection field for three different models: without any correction, with Hartree potential, and with both Hartree and exchange-correlation contributions. Compared to the zeroth order calculation, the Hartree correction lowers the height of the barrier because of the electric field continuity condition. The current is then increased up to one order of magnitude (from 0.16 mA to 2.17 A at $F_0 = 20\,\mathrm{kV.cm^{-1}}$). Moreover the 7.6 meV rise in the height of the barrier due to exchange-correlation effects makes the current to drop by one or two orders of magnitude. This clearly demonstrates how critical it is to consider those corrections in order to have a quantitative interpretation of such electronic transport regimes in THz QWIPs.

The inverse function of the high-field part ($\geq 8\,\mathrm{kV.cm^{-1}}$) of the circle-marked curve on figure 4 gives the $F_0(I)$ law that will be implemented in the model exposed in section II.

V. ANALYZE OF THE DISCONTINUITY LAW

This section is dedicated to giving a practical insight into the shape of the discontinuity law. A sample $\mathcal{D}$ law is implemented in the model in order to calculate the corresponding $V(i)$ curve. The macroscopic modifications induced by the modification of microscopic parameters are then analyzed. Figures 5 to 8 present different $\mathcal{D}$ laws and the corresponding current variations induced in the structure. The aim is to highlight the impact of each feature of the shape of the $\mathcal{D}$ law on the $V(i)$ curve. This work is fundamental to parameterize the upcoming optimization in section V.

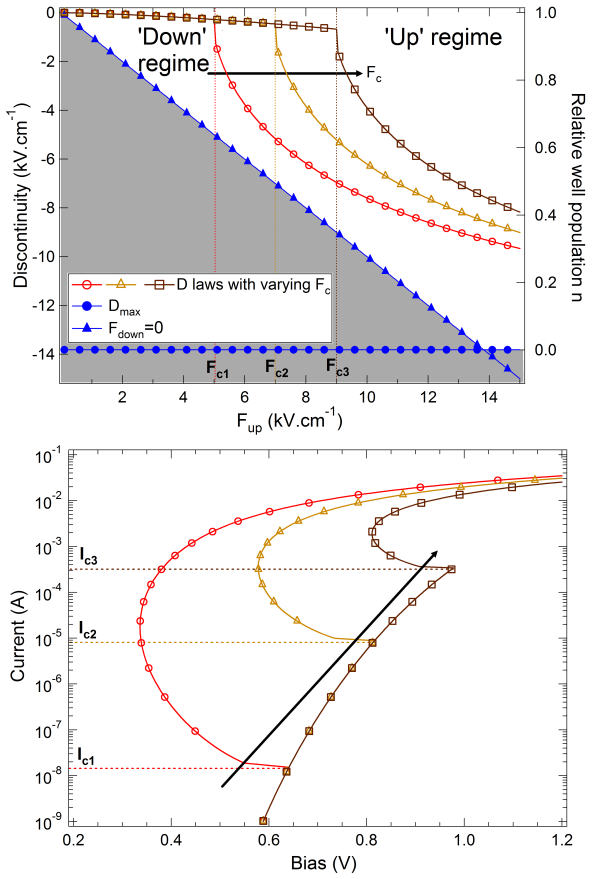

FIG. 5: Top: sample $\mathcal{D}$ laws with varying threshold fields F_c. The ionization degree of the well is given on the right axis. Bottom: corresponding $V(i)$ curves. The value of F_c sets the level of the transition current.

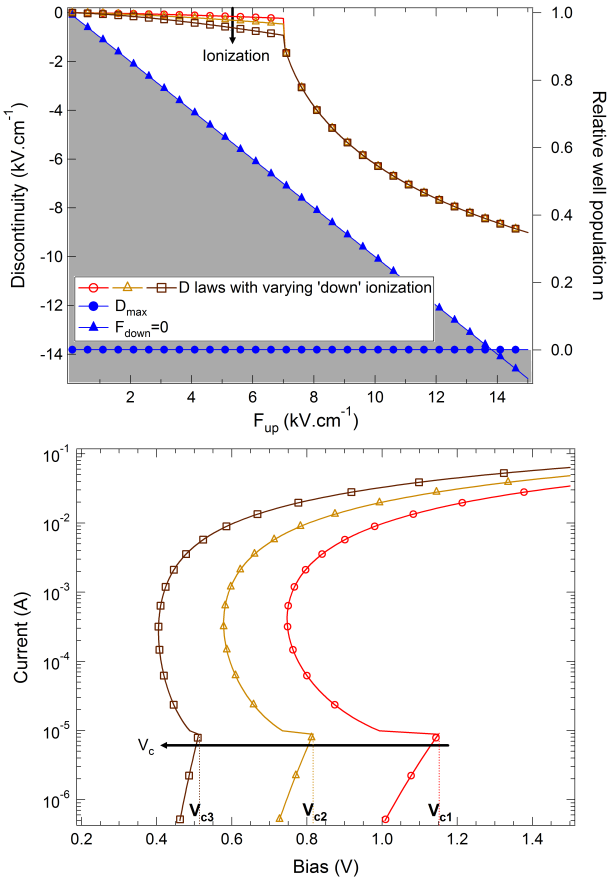

FIG. 6: Top: sample $\mathcal{D}$ laws with varying 'down' regime behavior. Bottom: corresponding $V(i)$ curves. The value of the threshold bias decreases when the wells are more ionized in the 'down' regime.

The 'up' and 'down' regimes are separated by the threshold field F_c. Below it, no electrons are present above the barriers, so the well is almost full, and the discontinuity is very small. For higher values of the upstream field, the well starts to be drained. If no capture mechanism is taken into account, the well will reach either of the following limit values. For low fields, the discontinuity is capped at a zero downstream field, in order for electrons to be extracted efficiently. For higher fields, the discontinuity cannot exceed the value given by a built-in charge equal to the doping amount in the well. These two values are labeled respectively $F_{down} = 0$ and $\mathcal{D}_{max}$ in figures 5 to 8. We will not consider the doping value as a varying parameter because its nominal amount has explained response peak in previous work[21].

Figure 5 shows that the current at the transition I_c goes up with the value of the threshold field F_c. The injection field value controls both the current flowing through the structure and the amount of energy acquired by the electrons of the continuum over the first period. It shall be noticed that the usual threshold fields are far below the value where the $F_{down} = 0$ and $\mathcal{D}_{max}$ straight lines cross.

Figure 6 shows that even in the down regime a positive charge in the wells has to be considered. Indeed, the bias at the transition V_c decreases when this 'down' ionization increases. If the $\mathcal{D}$ law is capped at zero, the structure will be rigid and strong bias modulations will occur. On the contrary at higher ionization levels the structure will look bent like a chain of pearls, and bias effects will be attenuated. At a given F_c this parameter directly sets the value of V_c.

Another interesting feature is the height of the transition, or more precisely the evolution of the relative distance between the $\mathcal{D}$ law and the $F_{down} = 0$ curves across and after the transition. Figure 7 proves that the 'S' pattern on the $V(i)$ widens when the 'up' ionization gets more effective. As a matter of fact if the relative distance shrinks to zero, the bias on the structure will only be the one applied upstream of the ionizing well. On figure 1, the 'S' is thin (0.18 V wide), which can be explained in two ways. Either a well at the end of the structure is strongly drained, or a well at the beginning of the structure is lightly drained. We already mentioned that ionization occurs on one of the first wells of the structure. This clearly advocates for a partial ionization of the wells.

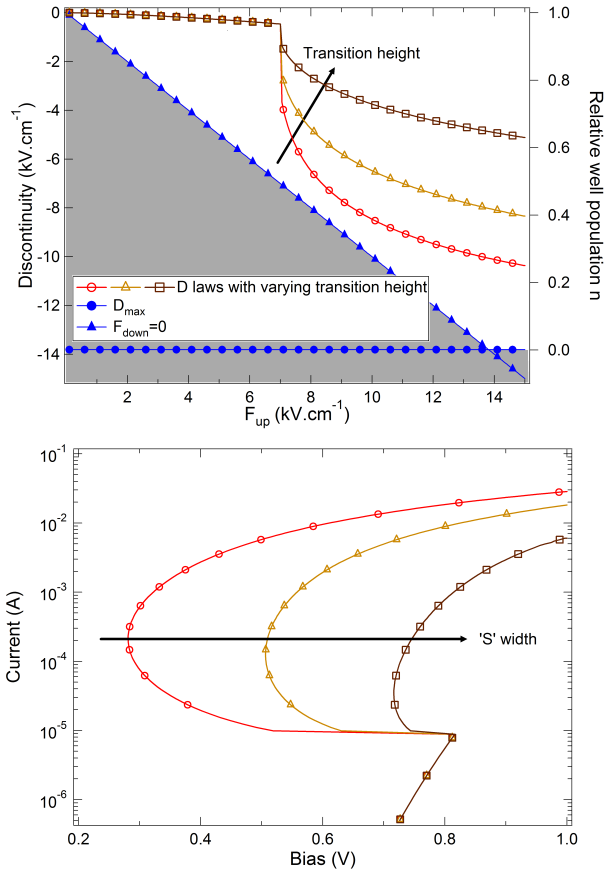

FIG. 7: Top: sample $\mathcal{D}$ laws with varying amplitudes of the drain at the transition. Bottom: corresponding $V(i)$ curves. A wide 'S' will follow an effective ionization of the wells.

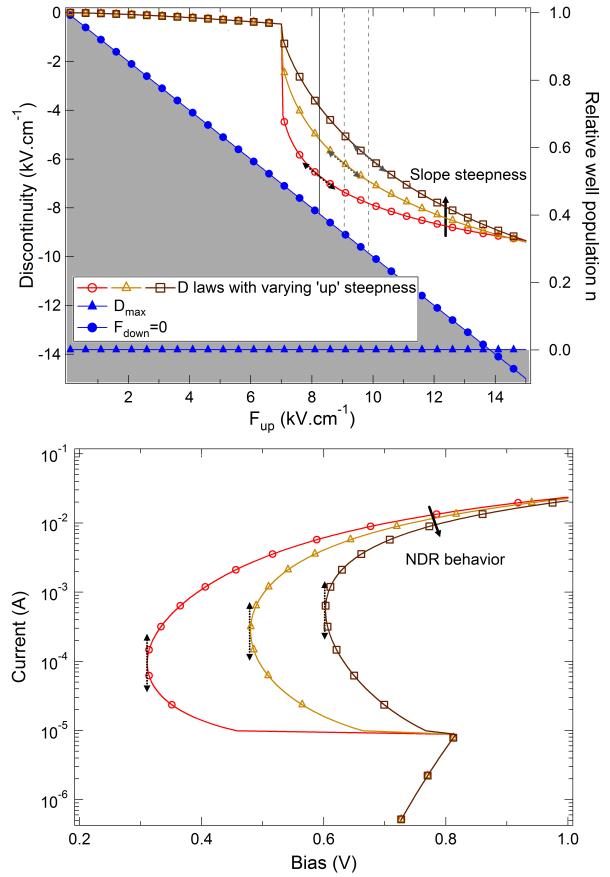

FIG. 8: Top: sample $\mathcal{D}$ laws with varying negative differential resistance thresholds. These are indicated by the -1 slope tangents. Bottom: corresponding $V(i)$ curves.

Figure 8 highlights the impact of the last critical parameter of the $\mathcal{D}$ law: the local slope. When it is inferior to -1 in the 'up' regime, an increase of the upstream field will cause a decrease of the downstream field. The structure is then in the negative differential resistance (NDR) regime. The rest of the 'S' pattern is shaped by the steepness of the $\mathcal{D}$ law.

VI. OPTIMIZATION AND DISCUSSION

The arguments of section IV prove that the $\mathcal{D}$ law features have quite uncorrelated effects on the $V(i)$ curve. This allows for a partially sequential resolution, much simpler than a raw multi-dimensional optimization, when trying to solve the functional equation (3).The fit of the experimental $V(i)$ in order to output an optimized $\mathcal{D}$ law uses the quasi-Newton method BFGS scheme[24]. Firstly the threshold field F_c is found by adjusting the transition current. Secondly the 'down' regime is calculated to fit the transition bias V_c. The third calculated parameter is the height of the transition, given by the width of the 'S' pattern. To finish with, the shape of the 'S' grants access to the rest of the 'up' regime shape of the $\mathcal{D}$ law. The main result given by this first model is that the well entering its regime transition is only partially ionized. As will be shown in figure 9 even at the highest field, the wells are barely half drained. A refill mechanism attributed to capture by LO phonon emission has to balance the draining process.

A model with a single $\mathcal{D}$ law for all the wells (as considered in section IV) cannot explain the $V(i)$ curve, and at the same time satisfy the impact ionization hypothesis. In this model the first well should be ionized first. The injection field should account for the amount of current at the transition (4.2×10^{-6} A), which gives $F_0 = 9.2\,\mathrm{kV.cm^{-1}}$. However it should also grant enough energy to electrons over the first period for impact ionization, which gives $F_0 \approx 11\,\mathrm{kV.cm^{-1}}$. This means that it is not the first well of the structure that gets ionized at this transition.

Another fact advocates for the ionization of several wells: the second cusp on the $V(i)$ curve of figure 1, at 0.72 V and 9×10^{-5} A. This cusp is the signature of another well entering its ionized regime. The band structure calculations of section III highlight the differences between the $\mathcal{D}$ laws of the first and the other wells. Figure 2 shows that at zero bias (a single Fermi level

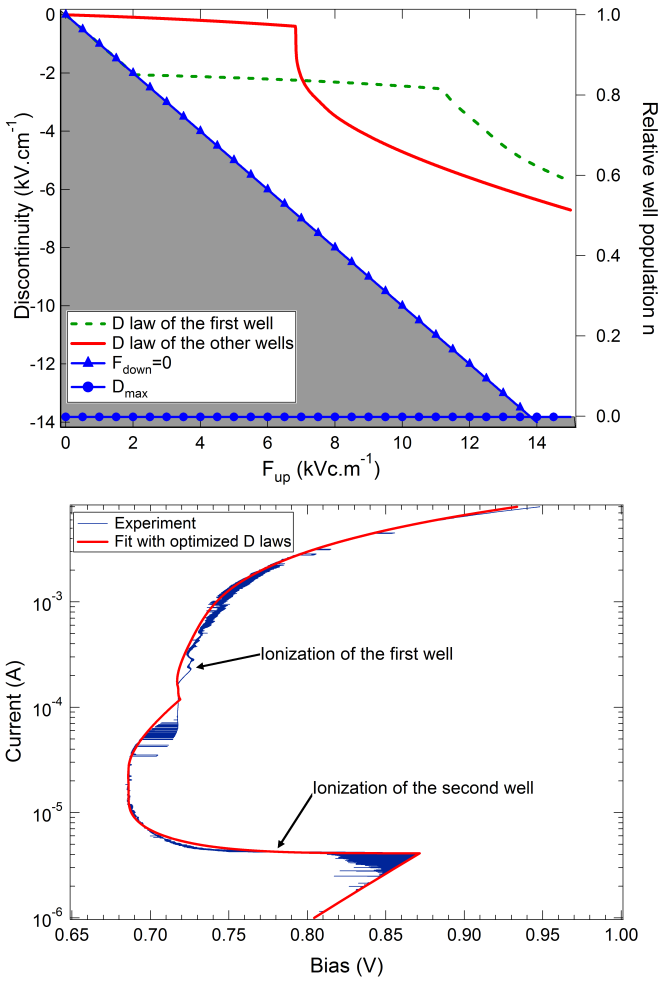

FIG. 9: Top: Adjusted $\mathcal{D}$ laws with the first well singled out. Bottom: Experimental and adjusted $V(i)$ curves.

throughout the whole structure), there is already a non zero injection field ($F_0(I)|_{0V} = 2.061\,\mathrm{kV.cm^{-1}}$). Due to quantum confinement, the first well will be more ionized than the other wells in the down regime, and its threshold field will be higher.

$$\begin{aligned} \mathcal{D}_{down}^{well\ 1} &= \mathcal{D}_{down}^{other\ wells} - F_0(I)|_{0V} \\ F_c^{well\ 1} &= F_c^{other\ wells} + F_0(I)|_{0V} + F_{eff} \end{aligned}$$

where $F_0(I)|_{0V} = 2.061\,\mathrm{kV.cm^{-1}}$ is the value of the injection field calculated at zero bias, and F_{eff} stands for the fact that all the electrons that can potentially ionize the first well are injected from the contact quasi Fermi level. On the other hand the remaining wells see not only electrons injected at the upstream well quasi Fermi level, but also electrons already flowing through the continuum over the barriers. We complete our model by considering two different $\mathcal{D}$ laws: one for the first well after the contact, and one for all the other wells.

Figure 9 shows the optimized $\mathcal{D}$ laws and the comparison between experimental and calculated $V(i)$. The latter shows an extremely good agreement, which should not be given too much credit: equation 3 has an infinite number of solutions. The sensitivity of the calculated $V(i)$ towards variations of the $\mathcal{D}$ laws is very acute next to the regimes-switch zone. Consequently the relevance of the adjusted $\mathcal{D}$ laws reaches its maximum around F_c. The good fit means that the objective of translating the information from the $V(i)$ to the $\mathcal{D}$ law curves has been fulfilled.

It shall be noticed that both the $\mathcal{D}$ laws of the first and other wells have the same shape, modulo the $\mathcal{D}_{down}$ and F_c translations. This ***renforcer*** the hypothesis that the process at stake is local. This is consistent with the same mechanism being responsible for the 'up' regime part in both cases: balance between well ionization and electron capture.

Note that the calculation of the output $\mathcal{D}$ laws is purely numerical, and does not rely on any physical assumption about the mechanism building up the charge. However the returned threshold field values exactly match the energy condition for intersubband impact ionization. For the first well, $F_c = 10.94 \pm 0.06\,\mathrm{kV.cm^{-1}}$ The ionizing electrons injected at the contact Fermi energy arrive with an energy of $E_c = 68\,\mathrm{meV}$ above the bound level. The energy condition for ionization $E_c > 2\Delta E = 64.5\,\mathrm{meV}$ is satisfied. For the second well at the transition, the threshold field value is $F_c = 6.83 \pm 0.03\,\mathrm{kV.cm^{-1}}$. In the hypothesis of a ballistic transport from the contact, this gives an incident energy of 103 meV above the bound level. Considering one LO phonon emission, the same energy condition $E_c = 67\,\mathrm{meV}$ arises. It is thus very likely that the mechanism responsible for the built-in charge effects that the regime transition in THz QWIPs is intersubband impact ionization. Further work will be published on these considerations about hot electrons kinetics.

In this sample, the second well of the structure will be ionized before the first one. In the latter case no NDR regime is observed. This counter-intuitive order of regime transitions highlights the critical importance of having a precise model of the contact. In Fig. 9, there is a small discrepancy in the shapes of the two $\mathcal{D}$ laws at the beginning of the 'up' regime part. When the first well begins to be ionized, the effective energy of the electrons arriving above the second well is increased, which downshifts the threshold field F_c) of the second well. In order to avoid complicating further the model by introducing another $\mathcal{D}$ law for the second well, we chose to add a small correction on the $\mathcal{D}$ law of the first well to keep a good fit of the $V(i)$.

Focusing back to the $I(v)$, it is possible to understand the asymmetry of the hysteresis pattern. When sweeping bias upwards, the breakdown of the second barrier drags along the first well into ionization. The third well is expected to be ionized at higher bias, out of the measurement range. When sweeping down the bias, the electric fields configuration allows the first well of the structure to shift to the 'down' regime without dragging along the

second one.

VII. CONCLUSION

We have shown that in THz QWIPs, the apparition of a built-in charge in the quantum wells generates drastic band structure rearrangements, which have been thoroughly investigated and successfully explained a regime transition in electronic transport. In particular the first wells of the structure are proven to be only partially drained at high electric fields. In the studied sample the second well enters its ionized regime before the first one. A precise 3D-2D model of the contact considering many-body effects highlights the difference in behavior between the first well and the other ones in the structure. Intersubband impact ionization has been identified as the probable origin of the built-in charge. Calculations of the $\mathcal{D}$ laws down from a quantum description are expected to give a good insight into the electron distribution in the continuum above the barriers, and thus raises interest in wavelengths broader than the THz spectrum.

Using the regime switch caused by impact ionization allows to optimize the design of very high sensitivity fast THz detectors. When the structure is polarized just below the threshold bias V_c, a few photons absorbed in the second well can trigger the shift to the 'up' regime. The main obstacle in the way of effective detectors is the fluctuations area near the transition, wherein the regime shift is not controllable. Understanding and deleting this area is the focus point for future work. Noise surge next to the instability is expected to be an issue, but the huge gain value (the current shifts by five orders of magnitude) soothes this concern.

APPENDIX

This appendix presents the numerical method used to solve the set of equations 5-9. The wave function of the well ground level is first calculated with a shooting method[25]. If V_{XC} is set to zero, equations 5-7 and 9 can be fused in the charge condition $\Theta(E_F, V_H) = 0$. Θ is a decreasing function of E_F, so a simple way to solve this equation is to find two E_F values where Θ is positive and negative, and use dichotomy. The key for the success of the method is the nature of equation 7 that allows to calculate the correction $V_H(z_i)$ thanks to the density at the previous step $n(z_{i-1})$. This is not possible while introducing the exchange correlation term. After getting a band structure $V^{(1)}(z)$ obeying to the Poisson equation (see figure 3), equation 8 gives the $V_{XC}^{(1)}$ correction. It is then input along $V^{(1)}(z)$ to recalculate the wave function and resolve $\Theta = 0$ to get $V^{(2)}(z)$. The result will be considered satisfactory as long as the change of the band structure in the second step is not significant: $V^{(2)}(z) \approx V^{(1)}(z) + V_{XC}^{(1)}$, which is always the case.

A similar method is used to calculate the band structure for any given value of F_0. The new criterion for the $\widetilde{\Theta}$ function is the value of the injection field. The 2D part of the problem is simplified: no calculations are made for the well area, except that its contribution to V_{XC} at zero bias is added to the 3D exchange-correlation potential. This slightly modifies the shape of the end of the barrier, and has a noticeable effect only at low fields when the barrier is not yet triangular.

[1] M. Tonouchi, Nature photonics **1**, 97 (2007).
[2] P. Siegel, IEEE Transactions on microwave theory and techniques **50**, 910 (2002).
[3] S. Dhillon, C. Sirtori, S. Barbieri, A. De Rossi, M. Calligaro, H. Beere, and D. Ritchie, Applied Physics Letters **87**, 071101 (2005).
[4] S. Kumar, B. Williams, S. Kohen, Q. Hu, and J. Reno, Applied Physics Letters **84**, 2494 (2004).
[5] S. Barbieri, P. Gellie, G. Santarelli, L. Ding, W. Maineult, C. Sirtori, R. Colombelli, H. Beere, and D. Ritchie, Nature Photonics **4**, 636 (2010), ISSN 1749-4885.
[6] S. Komiyama, O. Astafiev, V. Antonov, T. Kutsuwa, and H. Hirai, Nature **403**, 405 (2000), ISSN 0028-0836.
[7] T. Ueda, Z. An, K. Hirakawa, and S. Komiyama, Journal of Applied Physics **103**, 093109 (2008).
[8] D. Santavicca, B. Reulet, B. Karasik, S. Pereverzev, D. Olaya, M. Gershenson, L. Frunzio, and D. Prober, Applied Physics Letters **96**, 083505 (2010).
[9] P. Rauter, T. Fromherz, S. Winnerl, M. Zier, A. Kolitsch, M. Helm, and G. Bauer, Applied Physics Letters **93**, 261104 (2008).
[10] H. Luo, H. Liu, C. Song, and Z. Wasilewski, Applied Physics Letters **86**, 231103 (2005).
[11] L. Chang, L. Esaki, and R. Tsu, Applied Physics Letters **24**, 593 (1974), ISSN 0003-6951.
[12] K. G. McKay and K. B. McAfee, Phys. Rev. **91**, 1079 (1953).
[13] F. Capasso, W. Tsang, A. Hutchinson, and G. Williams, Applied Physics Letters **40**, 38 (1982).
[14] S. Dauwe, L. Mittelst "adt, A. Metz, and R. Hezel, Progress in Photovoltaics: Research and Applications **10**, 271 (2002), ISSN 1099-159X.
[15] A. Gomez, V. Berger, N. Péré-Laperne, and L. De Vaulchier, Applied Physics Letters **92**, 202110 (2008).
[16] H. Schneider and H. Liu, *Quantum well infrared photodetectors: physics and applications* (Springer Heidelberg, 2007).
[17] M. Ershov, V. Ryzhii, and C. Hamaguchi, Applied Physics Letters **67**, 3147 (1995).
[18] V. Ryzhii, Journal of Applied Physics **81**, 6442 (1997).
[19] L. Thibaudeau, P. Bois, and J. Duboz, Journal of Applied Physics **79**, 446 (1996).

[20] V. Jovanovic, P. Harrison, Z. Ikonic, and D. Indjin, Journal of Applied Physics **96**, 269 (2004).
[21] X. Guo, Z. Tan, J. Cao, and H. Liu, Applied Physics Letters **94**, 201101 (2009).
[22] O. Gunnarsson and B. Lundqvist, Physical Review B **13**, 4274 (1976).
[23] J. Demers and R. Maciejko, Journal of Applied Physics **90**, 6120 (2001).
[24] W. Press, S. Teukolsky, W. Vetterling, and B. Flannery, *Numerical recipes: the art of scientific computing* (Cambridge Univ Pr, 2007).
[25] P. Harrison, *Quantum wells, wires and dots: theoretical and computational physics of semiconductor nanostructures* (Wiley-Interscience New York, 2005).